Nuclear Engineering and Technology 53 (2021) 776–792

Contents lists available at ScienceDirect

Nuclear Engineering and Technology

journal homepage: www.elsevier.com/locate/net

Original Article

Design and operation of the transparent integral effect test facility, URI-LO for nuclear innovation platform

Kyung Mo Kim, In Cheol Bang*

Department of Nuclear Engineering, Ulsan National Institute of Science and Technology (UNIST), 50 UNIST-gil, Ulju-gun, Ulsan 44919, Republic of Korea

ARTICLE INFO

Article history:
Received 28 April 2020
Received in revised form
2 July 2020
Accepted 3 August 2020
Available online 15 August 2020

Keywords:
Integral effect test facility
Scaling analysis
Nuclear innovation
Nuclear safety
4th industrial revolution

ABSTRACT

Conventional integral effect test facilities were constructed to enable the precise observation of thermal–hydraulic phenomena and reactor behaviors under postulated accident conditions to prove reactor safety. Although these facilities improved the understanding of thermal–hydraulic phenomena and reactor safety, applications of new technologies and their performance tests have been limited owing to the cost and large scale of the facilities. Various nuclear technologies converging 4th industrial revolution technologies such as artificial intelligence, drone, and 3D printing, are being developed to improve plant management strategies. Additionally, new conceptual passive safety systems are being developed to enhance reactor safety. A new integral effect test facility having a noticeable scaling ratio, i.e., the (UNIST reactor innovation loop (URI-LO), is designed and constructed to improve the technical quality of these technologies by performance and feasibility tests. In particular, the URI-LO, which is constructed using a transparent material, enables better visualization and provides physical insights on multidimensional phenomena inside the reactor system. The facility design based on three-level approach is qualitatively validated with preliminary analyses, and its functionality as a test facility is confirmed through a series of experiments. The design feature, design validation, functionality test, and future utilization of the URI-LO are introduced.

1. Introduction

For the improved operation and emergency coping capability of nuclear power plants, innovative plant management technologies applying 4th industrial revolution technologies, such as big data processing [1], drone [2,3], artificial intelligence [4–6], 3D printing are being studied. Cho and Woo [2] investigated optimized motions of flying drones to encompass all areas of a nuclear power plant. For radiological monitoring and security analysis, the mechanics of drone was investigated, and specific motions of robot behaviors were simulated. Kim and Jang [3] developed robots that can operate under disconnected radio communication, while falling on uneven floors, and under loss of localization conditions such that they can be utilized under high radiation and in contaminated air. Oliveira and Almeida [4] developed a control system for a pressurizer using artificial intelligence to improve response time and operation reliability. Hagita et al. [5] developed a virtual reality system using a virtual survey meter for training in nuclear engineering. They examined the training to measure the change in radiation dose rate in various conditions to exhibit the validity and future applications of virtual reality. Santos et al. [6] demonstrated a virtual control desk for a research nuclear reactor to provide designers with a comprehensible human factor and verify human factor issues in the design of nuclear control desks. A control desk review and problem identification in the early design phase were provided in their study. Using 3D printing technology, many parts of the nuclear power plant, such as fuel, turbomachinery, and valve were fabricated to reduce cost and improve the mechanical strength. In addition, passive safety systems utilizing differentiated working principles are being developed to enhance reactor safety. Kim et al. [7] suggested integrated passive safety system (IPSS) to cope with SBO-combined accident. The passive safety injection and SG injection could be achieved by gravity with IPSS. Using MARS code, they obtained the IPSS strategy successfully ensure the safety during SBO-combined accident. Bang et al. [8] proposed passive in-core cooling system (PINCs) based on hybrid control rod-heat pipe, which combines functions of control rod and heat pipe to extend the accident coping time under SBO condition. Park et al. [9] investigated the feasibility of in-vessel retention of molten corium

* Corresponding author.
E-mail address: icbang@unist.ac.kr (I.C. Bang).

https://doi.org/10.1016/j.net.2020.08.006

Nomenclature

A	non-dimensional area [–]
a	cross-sectional area [m2]
Bi	Biot number [–]
Cp	Specific heat [kJ/kgK]
d	Diameter [m]
F	Friction number [–]
g	Gravity [m2/s]
h	heat transfer coefficient [kW/m2]
i	enthalpy [kJ/kg]
i_{fg}	latent heat of vaporization [kJ/kg]
U	Nondimensionalized velocity [–]
u	Velocity [m/s]
L	Nondimensionalized length [–]
l	Length [m]
N_{df}	drift-flux number [–]
N_{Fr}	Froude number [–]
N_{pch}	phase change number [–]
N_{sub}	subcooling number [–]
Pr	Prandtl number [–]
R	Richardson number [–]
St	Stanton number [–]
T	Temperature [K]
T*	Time ratio number [–]
Q	heat source number [–]
Z	Axial location [m]

Greek symbols

α	void fraction [–]
β	Volumetric expansion coefficient [1/K]
δ	Thickness [m]
τ	Nondimensionalized time [–]
θ	Nondimensionalized temperature [–]
ρ	density [kg/m3]

Subscript

f	liquid
g	gas
i	i-th
l	laminar
o	Reference
R	Relative
s	Solid
sub	subcooling
tur	turbulent

by external reactor vessel cooling with flooding of liquid metal. The performance of newly suggested passive safety systems including abovementioned systems and others under development for improvement of reactor safety, such as passive auxiliary feedwater system, safety injection with auto-depressurization, and passive containment cooling system must be evaluated by significant experimental and analysis works. Conventionally, new technologies have been developed through conceptual design, separate effect tests (SETs), numerical analyses utilizing computer codes, and integral effect tests (IETs). Although plant management using 4th industrial revolution technologies and newly suggested passive safety systems [7–9] can extensively innovate nuclear technologies, their technical quality is still far from those of real applications owing to insufficient validation studies in nuclear facility environments. Conventional IET facilities [10–18] have been designed to conserve the geometry of prototypes maximally (1/1 to 1/4 height ratio with respect to reference power plants) as summarized in Table 1, because they focus on the precise simulation of thermal–hydraulic phenomena and the system behavior of their reference power plant to analyze reactor safety under various postulated accident conditions. IET facilities enable reactor safety to be assessed based on design basis accidents, performance of passive safety systems, and numerical analysis capability of system analysis codes, such as RELAP5, TRACE, CATHARE, and MARS-KS. However, the large scale, complex geometry, and high cost of conventional IET facilities restrict the easy application and performance testing of the newly suggested technologies. A construction of micro IET facility, which appropriately simulates system behaviors and plant environments, will accelerate the improvement in the technical quality and feasibility of innovative technologies through easy applications and performance evaluations based on IETs.

Therefore, a new IET facility having large reduction ratio, "UNIST reactor innovation loop (URI-LO) was designed and constructed as a test bed for newly suggested technologies. The noticeable scaling ratio (1/8 height and 1/1152 vol scale with respect to APR-1400) of the URI-LO, compared to other IET facilities (1/4–1/1 height ratio), offers advantages in terms of research resources compared with other IET facilities. The main components of the URI-LO, which are manufactured using a transparent material (acrylic), enable the visualization of local phenomena inside the coolant system during transient conditions. Meanwhile, specific thermal–hydraulic phenomena inside conventional IET facilities, manufactured by metals, have been estimated by limited parameters, such as temperature, pressure, and flow rate, and separate effect tests under similar operating conditions. The visualization data of URI-LO would improve the understanding of thermal–hydraulic phenomena inside the PWR systems without additional separate effect tests or imagination about phenomena only based on numeric parameters.

The detailed utilizations of the URI-LO are summarized in Fig. 1:

Table 1
Design specifications of integral effect test facilities of worldwide.

Facility	Prototype	Volume scale	Height scale	Pressure scale	Scaling method
Semiscale [10]	Westinghouse PWR	1/1705.5	1/1	Full	Volumetric scaling
SPES-2 [11]	Westinghouse PWR	1/420	1/1	Full	Volumetric scaling
PKL III [12]	KWU PWR	1/145	1/1	Reduced	Volumetric scaling
BETHSY [13]	Framatome PWR	1/100	1/1	Full	Volumetric scaling
LOFT [14]	Trojan PWR	1/50	1/1	Full	Volumetric scaling
LSTF [15]	Westinghouse PWR	1/48	1/1	Full	Volumetric scaling
PUMA [16]	GE-SBWR	1/400	1/4	Reduced	Three-level approach
ATLAS [18]	APR1400	1/288	1/2	Full	Three-level approach
URI-LO	APR1400	1/1152	1/8	Reduced	Three-level approach

i) IETs regarding reactor safety issues; ii) performance tests on newly suggested passive safety systems; iii) manufacture of main components in the URI-LO, such as the reactor pressure vessel, cold leg, hot leg, safety injection tanks, and steam generators using transparent material, which can provide visual observations of local phenomena inside the coolant system during transients. The visual data would clarify many complex phenomena and extend the utilization of the facility; iv) several parts of the facility can be easily replaced with 3D-printed parts to examine the feasibility of 3D printing technology on nuclear power plants; v) demonstration of facility operation to public members, students, and nuclear-related workers can improve public acceptance on nuclear energy.

As listed, the URI-LO is expected to be a powerful test bed for new innovative technologies with various roles, including a thermal–hydraulic integral effect test facility and an educational tool. This paper presents the detailed design of the URI-LO and a qualitative design validation based on preliminary analysis results (two postulated accident conditions. reactor coolant pump (RCP) rotor seizure, and station blackout (SBO)) using the MARS-KS thermal–hydraulic system code.

2. Design of the URI-LO

The URI-LO is a scaled-down IET facility of APR-1400 designed based on a three-level scaling methodology suggested by Ishii and Kataoka [19] to conserve the thermal–hydraulic phenomena and system behavior of reference power plants. A detailed design process including the determination of the scaling methodology, scaling ratios, and expected scaling distortions are described in this section with an introduction of the overall design features of the URI-LO.

2.1. Scaling analysis

Conventional IET facilities have been designed based on the following representative scaling analysis methodologies: Linear scaling [20], volumetric scaling [21], and three-level scaling methods [19]. Although the linear scaling method involves a relatively simple scaling process that maintains the diameter and length ratios of a reference model, its simulation capacity of thermal–hydraulic phenomena in prototypes is degraded because the conservation of velocity in a reduced time scale distorts the acceleration term. The distortion of the acceleration would fatally distort the force balance dominating the hydraulic behaviors. The volumetric scaling method simulates the system behavior of a prototype in real time by preserving the core power ratio and volume ratio. The real-time simulation of IET facilities, designed using the volumetric scaling method, is advantageous for IETs; however, the larger surface area to volume ratio than prototype induces scaling distortions in terms of heat source and sink. Additionally, the full height conservation of the reference model according to volumetric scaling method limits the design criteria of the scaled-down facility and reduces the similarity of multidimensional phenomena in specific components. The three-level scaling approach, suggested by Ishii and Kataoka [19], conserves the thermal–hydraulic phenomena of the reference system, thereby supplementing the disadvantages of linear and volumetric scaling methods. In this approach, the scaling ratio of the height and diameter can be varied, and a reduced height provides good similarity on multidimensional phenomena. Therefore, the three-level scaling approach was utilized in the scaling analysis of the URI-LO, in which a significantly reduced height scale was necessitated due to given limitation of space or size of a facility. The three-level scaling approach is a top-down scaling method involving the following design steps: i) integral system scaling, which matches the nondimensional numbers deduced by single-phase and two-phase flow governing equations of prototypes and scaled facilities; ii) control volume scaling, which scales inventories of mass and energy of components while considering boundary flow scaling; iii) local phenomena scaling, which considers the conservation of specific phenomena inside systems, such as flow instability, break flow, flow regime, and critical heat flux. Based on the three-level scaling approach, scaling analyses of the URI-LO were conducted. In cases where the design parameters determined in individual design steps conflicted each other, integral system scaling was performed prior to other design steps.

APR-1400, which is a pressurized water reactor (PWR) design of the Korean hydro and nuclear power (KHNP), was selected as a reference power plant for the URI-LO because it is the most advanced and recent PWR design. Consequently, various innovative

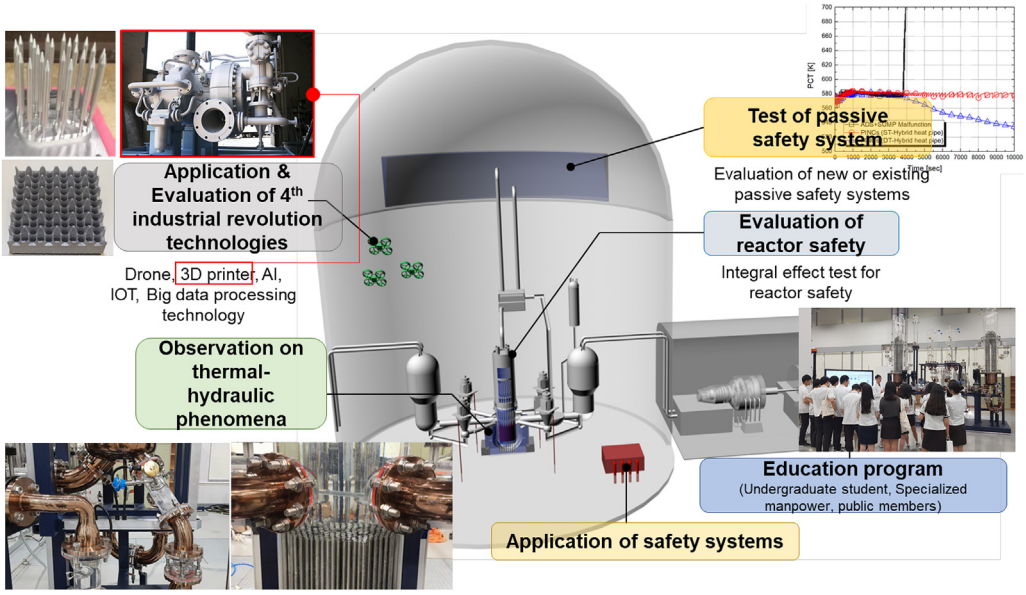

Fig. 1. Introduction on utilization of URI-LO.

technologies can be applied. Therefore, a three-level scaling analysis was conducted using the APR-1400 design information and predetermined scaling ratios.

For single-phase natural circulation, the mass, momentum, and energy conservation equations regarding fluid and solid are non-dimensionalized with boundary conditions based on the three-level scaling approach. By nondimensionalizing the governing equations, dimensionless numbers (e.g., the Richardson and Stanton numbers) as well as the time ratio number, heat source number, and Biot number, which represent thermal–hydraulic phenomena, are deduced. Preservation of the deduced nondimensional numbers is crucial for conserving the thermal–hydraulic phenomena of the reference model with a scaled facility. Therefore, the scaled-down model was designed to satisfy the conditions expressed from Eqs. (1)–(6).

$$R_R = \left(\frac{\beta g \Delta T_o l_o}{u_o^2}\right)_R = 1.0 \tag{1}$$

$$St_{iR} = \left(\frac{4hl_o}{\rho C_p d u_o}\right)_R = 1.0 \tag{2}$$

$$T_{iR}^* = \frac{l_R}{u_R \delta_{iR}^2} = 1.0 \tag{3}$$

$$Q_{siR} = \frac{(\rho C_p)_R d_{lR}}{\delta_{oR}} = 1.0 \tag{4}$$

$$B_{iR} = h_R \delta_{iR} = 1.0 \tag{5}$$

$$\left(\sum_i F_i / A_i^2\right)_R = 1.0 \tag{6}$$

$$F_i = \left(\frac{fl}{d} + K\right)_i \tag{7}$$

The scaling ratios of the URI-LO in term of length and diameter were 1/8 and 1/12, respectively. Based on calculation results about the reference velocity of the facility having various length ratios under same diameter ratio condition, the length ratio of 1/8, which shows equal reference velocity with the prototype, was determined. To simulate the system behavior under the high-pressure and high-temperature condition of the reference power plant with reduced pressure condition (owing to the mechanical strength of the transparent material), scaling analyses were conducted based on the thermal–hydraulic properties of the simulant fluids. The Richardson number, which represents the relation between natural convection and forced convection, was matched by controlling the system pressure loss with installations of appropriate orifices in the flow paths. The time ratio and heat source numbers were preserved by matching the flow velocity and solid thickness of the components. The Stanton and Biot numbers are indicators of energy conservation that are affected by heat transfer coefficients. Different thermal–hydraulic properties between the reactor coolant and simulant fluid of the reference model and the URI-LO distort the heat transfer coefficients, and hence the Stanton and Biot numbers. Therefore, the degrees of scaling distortion in terms of energy conservation were analyzed in detail.

For a scaling of two-phase natural circulation, similarity groups, characterized by kinematic, dynamic and energy similarities, were developed from perturbation analysis based on the one-dimensional drift flux model. The important dimensionless numbers include phase change number (Zuber number), subcooling number, Froude number, and Drift flux number as expressed by Eqs (8)–(11). In addition, the relative dimensionless numbers must be matched as arranged from Eqs (12)–(14).

$$N_{pch} = N_{Zu} \equiv \left(\frac{4q_o''' \delta l_o}{d u_o \rho_f i_{fg}}\right)\left(\frac{\Delta\rho}{\rho_g}\right) \tag{8}$$

$$N_{sub} \equiv \left(\frac{i_{sub}}{i_{fg}}\right)\left(\frac{\Delta\rho}{\rho_g}\right) \tag{9}$$

$$N_{Fr} \equiv \left(\frac{u_o^2}{g l_o \alpha_o}\right)\left(\frac{\rho_f}{\Delta\rho}\right) \tag{10}$$

$$N_{df} \equiv \left(\frac{V_{gj}}{u_o}\right)_i \tag{11}$$

$$(N_{Zu})_R \equiv \left(\frac{q_o''' \delta l_o}{d u_o \rho_f i_{fg}}\right)_R \left(\frac{\Delta\rho}{\rho_g}\right)_R = 1 \tag{12}$$

$$(N_{sub})_R \equiv \left(\frac{i_{sub}}{i_{fg}}\right)_R \left(\frac{\Delta\rho}{\rho_g}\right)_R = 1 \tag{13}$$

$$(N_{Fr})_R \equiv \left(\frac{u_o^2}{l_o}\right)_R \left(\frac{\rho_f}{\Delta\rho}\right)_R = 1 \tag{14}$$

Table 2
Thermal-hydraulic properties and scaling factors [22].

Fluids	Density ratio	Boiling point [K]	*Pr*	u_R	$h_{R,lam}$	$h_{R,tur}$
Water	90.4	485.5	0.88	–	–	–
R134a	89.7	275.1	3.95	0.84	1.69	2.14
R123	89.2	329.1	4.60	1.00	1.25	2.42
R600a	90.8	289.2	4.34	1.10	1.72	1.04
FC-72	94.0	339.2	8.83	0.84	0.94	2.42

If the fluid property of the scaled model was equal to that of prototype, velocity ratio and time ratio is inversely proportional to square root of length ratio according to Eq. (14), because ratio between liquid density and density difference between liquid and vapor is nearly unity. The substitutions of velocity ratio and time ratio of two-phase flow to single phase flow geometric scale requirements achieve same similarity requirement. However, the fluid properties of URI-LO differ from prototype. Therefore, velocity and time scales in single phase flow condition were distinguished from those of two-phase flow condition.

Table 2 summarizes the thermal–hydraulic properties and flow parameters of water (reactor coolant of prototype) and several refrigerants (simulant fluid candidates of the test facility). The density ratio of the simulant fluid in a relatively low-pressure and low-temperature condition was similar to that of high-pressure water. The match in density ratio between the liquid and vapor of fluids is a priority for conserving two-phase flow (void fraction and bubble size) characteristics. After determining the operating pressure (by matching the density ratio between liquid and vapor with that of prototype) of the facility according to simulant fluid, operating temperature was determined by matching subcooling number. Based on thermal-hydraulic properties such as density, specific heat, viscosity, and thermal conductivity of the operating pressure and temperature, relative velocities and Reynolds numbers were calculated. The relative heat transfer coefficients for laminar and

Table 3
Global scaling results for single-phase natural circulation of URI-LO [22] (* initial parameters, ** secondary parameter determined by initial parameters, *** Global scaling parameters by initial and secondary parameters).

Parameters	Scaling ratio	URI-LO
Length (height)*	l_{oR}	1/8
Diameter*	d_{oR}	1/12
Core temperature rise*	dT_{oR}	1/2
Velocity**	$((\rho c_p)_R)(l_{oR})^{1/2}$	1/1
Time**	$((1/\rho c_p)_R)(l_{oR})^{1/2}$	1/8
Richardson number***	1.0	
Friction number***	1.0	
Time ratio number***	0.84	
Stanton number (laminar)***	0.66	
Stanton number (turbulent)***	0.50	
Biot number (laminar)***	0.80	
Biot number (turbulent)***	0.64	
Heat source number***	0.72	

turbulent regions were finally analyzed. As shown in the table, the flow velocity can be conserved by the refrigerants in a reduced facility owing to differences in thermal–hydraulic properties, whereas the heat transfer coefficients were notably distorted. The laminar heat transfer coefficients of R123 and FC-72 were similar with that of water, whereas the Prandtl number differed vastly for the distortion in turbulent heat transfer coefficient between the water and simulant fluid candidates. Consequently, FC-72 was selected as a simulant fluid for the URI-LO after comprehensively considering the boiling temperature (high boiling temperature of simulant fluid induces the thermal deformation of transparent materials (>80 °C)), compatibility with material (chemical reaction between coolant and transparent material), and degrees of scaling distortions in terms of reference velocity and heat transfer coefficients. The remarkable distortion in the turbulent heat transfer coefficient was preserved by adjusting the heat transfer areas of the heater and steam generator u-tube. The overall scaling ratios and global scaling parameters for the single-phase natural circulation of the URI-LO are listed in Table 3.

In the two-phase flow scaling analysis, relative nondimensional numbers including the phase change, subcooling, Froude, drift–flux, friction, and orifice numbers were deduced from one-dimensional drift–flux model, and transfer functions were analyzed. Furthermore, URI-LO design has effort to have nondimensional numbers as unity. For the scaling analysis of the boundary, inventory, and local phenomena after a global scaling analysis, the experimental ranges were determined because all local phenomena inside the reference model could not be accurately simulated by the URI-LO that was operating at a low pressure and low temperature.

The URI-LO was designed to be operated using a simulant fluid, FC-72, to simulate the system behaviors of the reference model at a relatively low pressure and low temperature. Because of the specific operating condition of the facility, several thermal–hydraulic phenomena could not be precisely simulated. The representative specific phenomenon considered in various postulated accident conditions is the critical flow. Therefore, the design basis accidents, such as loss of coolant accident, main steam line break, and steam generator u-tube rupture that were primarily affected by the critical flow (break flow) were excluded from the experimental range of the URI-LO. Excluding the postulated accidents accompanying the critical flow, three transient conditions were selected as the target experimental conditions of the URI-LO:

(1) reactor coolant pump (RCP) rotor seizure accident,
(2) prolonged station blackout (SBO),
(3) total loss of feedwater (TLOFW) accident.

Although the loss of flow in the reactor coolant system (RCS) is more frequently considered in PWRs, RCP rotor seizure accident was selected because the RCP rotor speed of the facility was insufficient to fully follow the coastdown curve of the reference RCP. The coastdown curve in the flow rate range close to steady state condition can be appropriately simulated with RCPs of the facility, while RCP rotor speed is hard to control at the very low flow rate conditions. In addition, variations of RCS pressure and minimum departure from the nucleate boiling ratio (mDNBR), those are main system behaviors considered in RCP rotor seizure accident, occurs early phase of transient (period that coastdown curve could be simulated) owing to dramatic decrease of RCS flow. Therefore, RCP rotor seizure accident was considered as transient condition of the facility. During the RCP rotor seizure accident, the pressure of = RCS and mDNBR are main safety criteria; hence, the scaling design of local phenomena focusing on the departure from the nucleate boiling ratio (DNBR) was performed. In addition, prolonged SBO was determined as a reference condition for testing the performance of newly suggested safety systems and innovative technologies. Inventory scaling and energy scaling design to conserve the discharge of reactor and steam generator coolants, variation in system pressure, and fuel cladding temperature during prolonged SBO was conducted. In a TLOFW condition, the discharge of steam generator coolant, operation of safety injection pumps and tanks according to the feed and bleed strategy, and peak cladding temperature are key parameters in safety analysis. Consequently, the inventory of emergency cooling tanks and steam generators as well as the injection flow rate were scaled. Injection mass flow rate curve was calculated based on differential pressure between RCS and SITs, and the curve was shifted to preserve that of prototype by installation of orifices. After scaling analysis on injection flow rate, the inventory of SITs was especially scaled, because different scaling ratios of volume scaling ratio ($(D^2L)_R$) and flow area scaling ratio ($(D^2)_R$) results in different inventory variation behavior compared to prototype.

2.2. Design feature of URI-LO

According to the abovementioned scaling analysis, the URI-LO was designed and constructed to with a 1/8 height ratio and 1/12 diameter ratio (1/1152 vol ratio). The total height and width of the URI-LO were 3.8 and 4.04 m, respectively. Fig. 2 shows an overall design feature of the URI-LO; Fig. 3 shows a photograph of the constructed URI-LO.

The RCS comprises a reactor pressure vessel with a downcomer, heater (fuel rod) assembly of maximum heat capacity 200 kW, pressurizer, two hot legs, four cold legs (four intermediate legs with loop seals), and four RCPs. The heater (fuel rod) diameter and pitch to diameter ratio (P/D) were equivalent to those of the reference power plant, and the height was reduced by 1/8. A total of 396 heaters were installed inside the reactor pressure vessel, and the number of heaters was determined to preserve the scaling distortion effect of the heat transfer coefficient attributed to the different thermal–hydraulic properties of the simulant fluid and water. The heaters divided into six groups (66 fuel rods/group) in radial direction to control the radial power distribution. The maximum heat capacity of the heater assembly, which corresponded to 2% of the reference model's full power, exhibited a decay heat trend under transient conditions. The embedment of a flow skirt between the downcomer and inner shell of the RPV altered the pressure drop and homogeneous flow distribution in the radial direction. Across the pipeline of the RCS, which was represented by the cold, intermediate, and hot legs, orifices were included for flow behavior simulation. Azimuthal angles of the cold legs and hot legs were preserved with those of prototype. Based on pressure drop

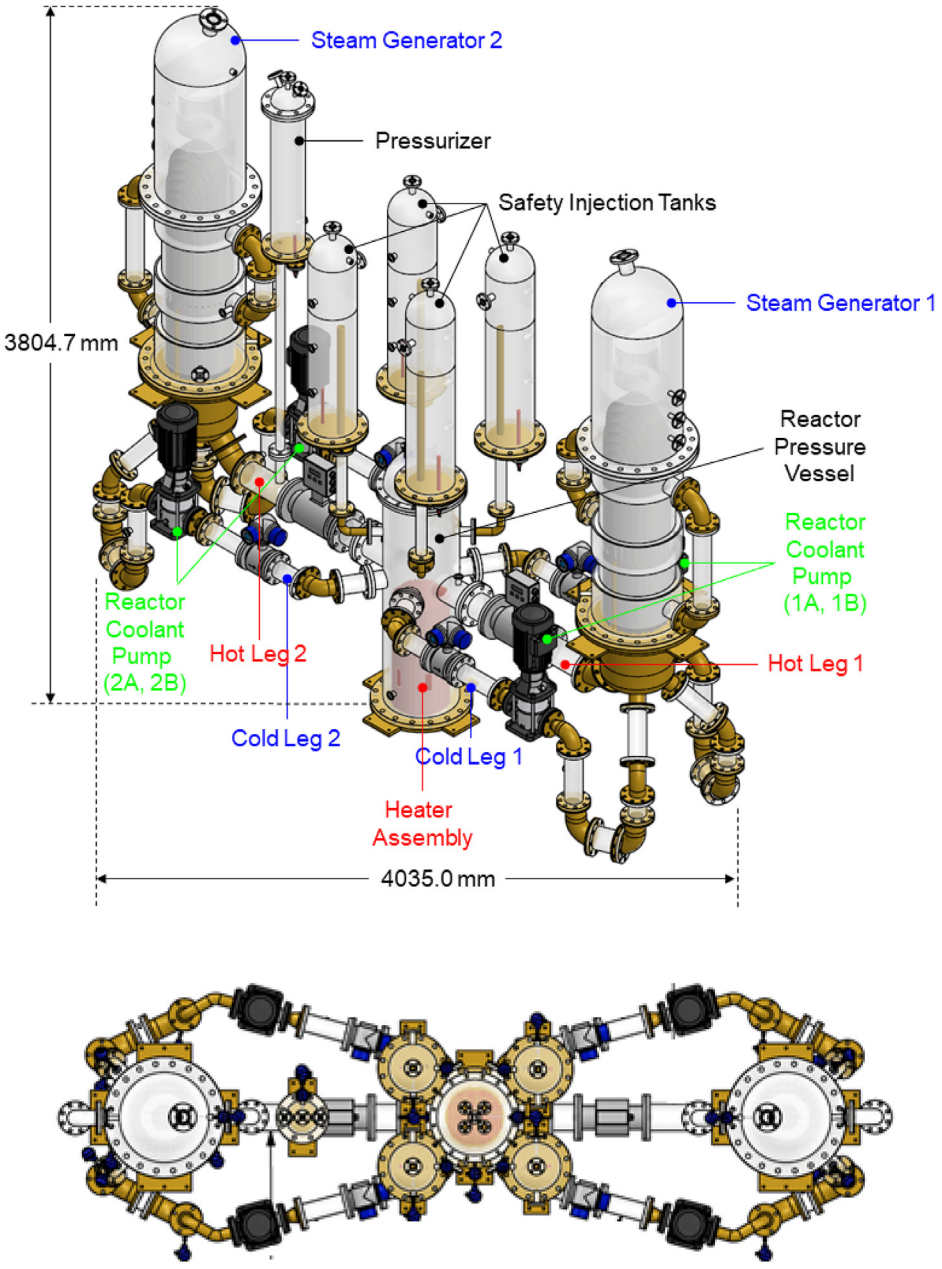

Fig. 2. Detail design drawings of URI-LO [22].

calculation across the primary system, RCPs having maximum efficiency at flow rate of normal operation were installed. The RCPs have convertor and PID controller to vary the flow rate by controlling the RCP rotor speed.

The safety injection tanks comprise a container, heater, pressure valve, and standpipe having holes at the bottom side of the tank simulating fluidic device installed with a direct vessel injection (DVI) line as a fundamental passive safety system. Although original fluidic device of SITs utilizes the vortex effect with control flow of tangential direction to control the injection flow rate according to tank level, standpipe having holes in tangential direction of supply flow was primarily installed because quantitative scaling design of fluidic device is hard. Two steam generators comprising u-tubes, a steam dryer, a steam separator, a main feedwater system with a recirculation pipeline, and an auxiliary feedwater system were constructed. The number of u-tubes was adjusted to preserve the energy scaling distortion effect in the heater design, because the relative heat transfer coefficient (heat transfer coefficient ratio of simulant fluid to reference) is highly distorted as presented in Table 2 due to different properties. The steam generators were designed to have feedwater lines to economizer and downcomer. Feedwater pumps were determined by same design process of RCPs. At the middle of feedwater lines to economizer and downcomer sections, isolation valves were installed for the purpose of main feedwater isolation and simulation of loss of feedwater condition. Pressurizer (PZR) was connected to the hot leg of a loop with surge line. The PZR was designed to have safety depressurization system nozzle, spray nozzle, and venting nozzle at the top with heater at the bottom side for the pressure control of RCS. The system pressure and flow control system will comprise a pilot-operated safety relief valve (POSRV) at the top of the pressurizer, main steam safety valves (MSSVs) at the middle of the main steam

Fig. 3. Photo of constructed URI-LO.

line, main steam isolation valves (MSIVs), and main feedwater isolation valves. The POSRV, which would be operated between upper and lower pressure boundaries (110% and 90% of RCS pressure of normal operation condition), was designed to be located between safety depressurization system nozzle and container acting as PZR relief tank. Total 6 MSSVs (three valves for each loop), which was designed to be located at the middle of the main steam line, will be connected to separate vacuum chamber owing to subatmospheric operating condition of secondary system of the facility.

Several parts, including the curved pipelines, fuel alignment, control rod drive mechanism (CRDM) housing, and spacer grid with mixing vane are difficult to fabricate or have multiple welding parts; therefore, they are currently manufactured using stainless steel. However, the abovementioned components will be replaced by 3D-printed items. Except the stainless-steel parts (yellow parts of Fig. 2), most components were manufactured using transparent materials (acrylic) for the visualization of thermal–hydraulic phenomena and system behaviors under various operating conditions. The instrumentations for measurement of fluid temperatures and pressures were depicted in Fig. 4. A total of 67 thermocouples (40 TCs for fluid temperature and 27 TCs for heater), 16 pressure transducers, and 12 mass flowmeters (turbine flowmeter for simulant fluid and electric flowmeter for water) were used to measure the temperature, system pressure, differential pressure, and flow rates in the entire system. The detail numbers and uncertainties of instrumentations were summarized in Table 4. The combination of numerical data obtained using digital and analog instruments and visualization data will provide a comprehensive understanding of multidimensional behaviors and complex thermal–hydraulic phenomena related to multiphase flows inside the system. In particular, multidimensional phenomena, such as flow regimes, countercurrent flows, and RCP loop seal clearing are difficult to observe at conventional IET facilities owing to similar length and diameter scaling ratios [11].

3. Preliminary analysis for design validation of URI-LO

To confirm the similarity of system behaviors of the facility's reference power plant, preliminary analyses using a multidimensional analysis for reactor safety (MARS) code were performed for design validation. Two RCP rotor seizure accidents and station blackouts were analyzed in this study. Short- and long-term system behaviors with key safety parameters were compared with safety analysis and IET results of facilities having the same reference model. Preliminary analyses were conducted based on using water as a coolant of the URI-LO; therefore, variations in system parameters were compared quantitatively in this phase to observe the simulatability of the designed facility.

3.1. Analysis method and steady state

The MARS nodalization of hydraulic volumes, boundary conditions, and heat structures (heat transfer boundary) of RCS and

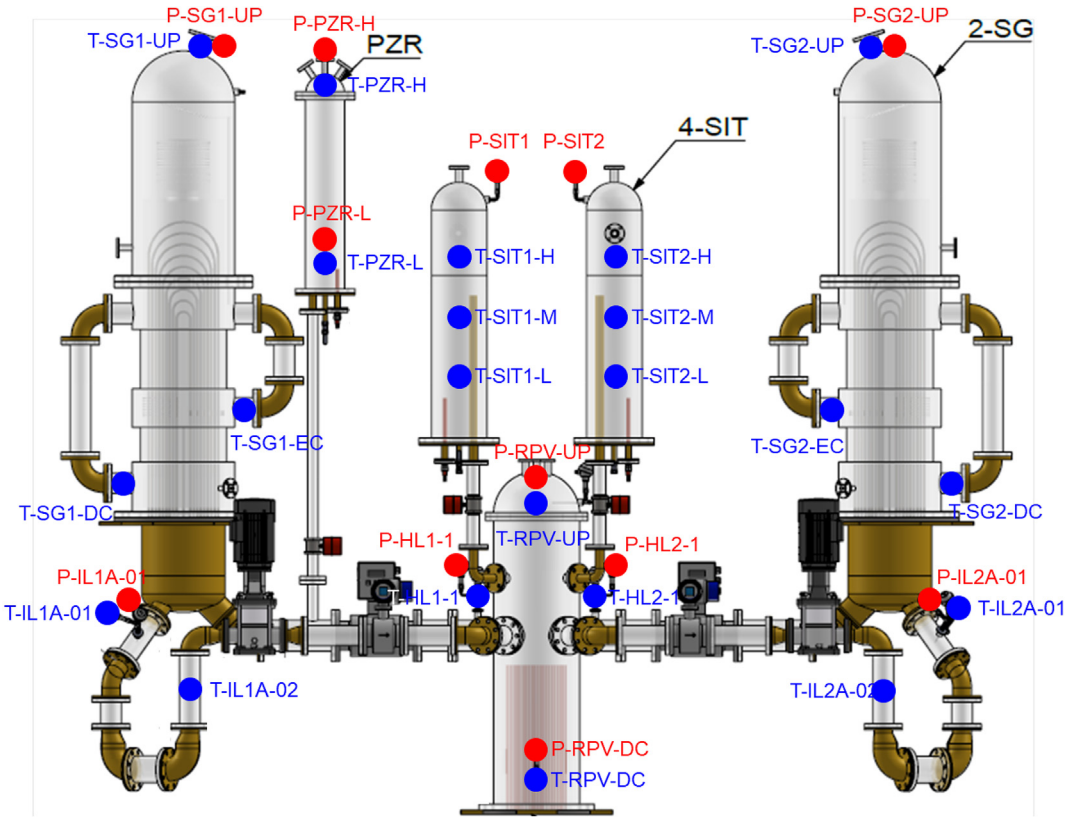

Fig. 4. Locations of thermocouples and pressure sensors for measurement of fluid temperature and system pressures.

Table 4
Numbers and uncertainties of measurement instrumentations.

Sensors	RPV	Loops	SITs	PZR	SGs	Uncertainties
Thermocouples (heater)	20	–	4	1	–	±0.5 °C
Thermocouples (Fluid)	10	10	12	2	6	±0.1 °C
Pressure sensors (absolute)	2	6	4	2	2	±0.1 kPa
Flowmeters (mass flow rate)		6	4		2	±0.01 kg/s

secondary systems was modeled as shown in Fig. 5. The hydraulic volume of the reactor pressure vessel comprised a low plenum, an average channel, a hot channel, a downcomer, a flow distributor between the downcomer and average channel, an upper plenum, and an upper head; these components were categorized into pipe, single volume, and branch components. The downcomer section was modeled by an annulus component to appropriately analyze three-dimensional phenomena including asymmetric system behaviors. Heater assemblies serving as fuel assemblies, heaters inside the pressurizer and safety injection tanks, and steam generator u-tubes were modeled by the heat structure (heat sources and heat exchange boundary condition). The adiabatic condition was assumed in the hydraulic volumes excluding the heat structure parts because acrylic has a low thermal diffusivity and the facility was operated at low temperatures. To control the system pressures and flow rates, a valve system comprising a POSRV, MSSVs, MSIVs, and MFIVs was additionally modeled to be operated at predetermined open/close boundaries. The main feedwater, auxiliary feedwater, and main steam were simulated based on appropriate pressure and flow boundary conditions using time-dependent junctions and volumes.

For the various IETs, a steady-state normal operation condition of the reference model must be achieved. The scaling ratios, global scaling parameters, and thermal–hydraulic properties of the selected simulant were deduced from the scaling analysis, whereas the normal operating condition of the URI-LO was determined as presented in Table 5. The operating condition corresponded to 2% of the full power operation condition of the prototype; therefore, system behaviors from the initial phase of the transient condition were observed. As summarized in Table 5, the URI-LO was operated at a reduced pressure, an increased core temperature, the core power, the coolant flow rate, and the coolant temperature condition with the scaling ratios. In a test run using water as a coolant, the core temperature increase was used as a standard for determining the steady-state condition.

The normal operating conditions (system flow rates, pressures, temperatures, quality distribution according to elevation of steam generators; and heat balances between primary and secondary systems) of the test run in Table 5 was successfully calculated within 2% deviations.

3.2. Two RCP rotor seizure accidents

The RCP rotor seizure accident enables observations of asymmetric behaviors according to loops having intact and malfunctioning pumps, as well as variations in RCS pressure and mDNBR in short-term transients. Two RCP rotor seizure accident was selected as a representative transient scenario of the facility because it can confirm the simulatability of the URI-LO in terms of short-term transient behaviors. The preliminary analysis of RCP rotor seizure accident of URI-LO in this paper was conducted with utilization of water as reactor coolant. In a condition that a single RCP rotor seizure occurs, variations of representative system behaviors (mDNBR and RCS pressure) are indistinctive because time scale is reduced due to reduction of geometry. For remarkable observations

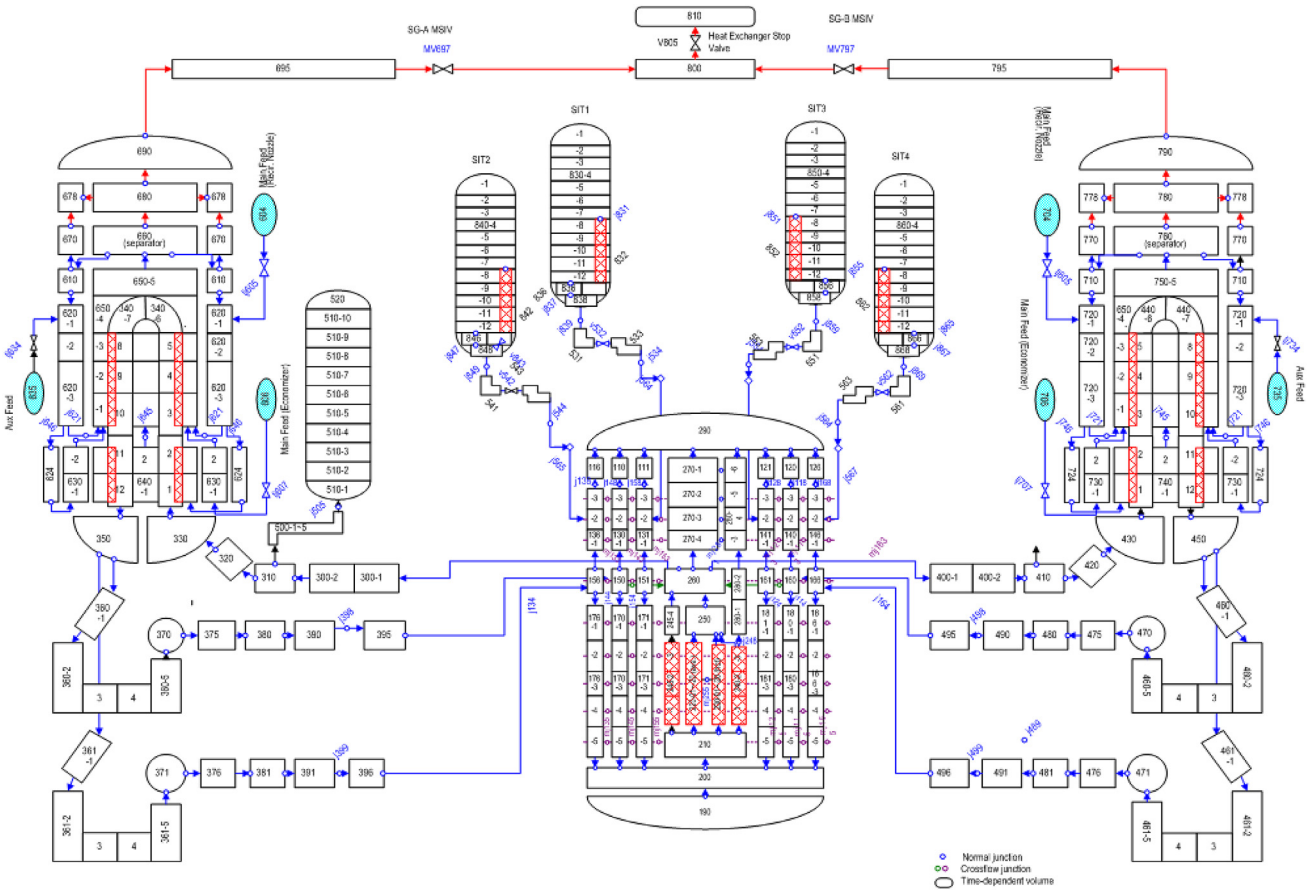

Fig. 5. MARS nodalization of URI-LO.

Table 5
Determined normal operating condition of URI-LO [22].

Design parameter	APR-1400	Scaling ratio (P/M)	URI-LO (FC-72)	URI-LO (water)
Primary system pressure [bar]	155.1	77.6	2.0	1.0
Core inlet temperature [K]	563.7	–	305.2	347.2
Core outlet temperature [K]	598.1	–	339.6	364.4
Core temperature difference [K]	34.4	1.0	34.4	17.2
Core flow rate [kg/s]	550.6	$c_{p,oR}l_{oR}^{1/2}d_{oR}^{1/2}$	5.4	2.7
Core power [MW]	79.8	$l_{oR}^{1/2}d_{oR}^{1/2}$	0.196	0.196
SG pressure [bar]	70.0	583.3	0.12	0.24
SG steam temperature [K]	564.1	–	313.2	339.2
SG Heat removal rate/ea [MW]	39.92	$l_{oR}^{1/2}d_{oR}^{1/2}$	0.098	0.098

on the system behaviors, two RCP rotor seizure accident was analyzed. The single RCP rotor seizure condition of reference power plant will be analyzed in the future with implementation of properties of simulant fluid to the code. The general phenomena inside the RCS during the RCP rotor seizure accident were as follows: (1) dramatic decrease in RCS flow; (2) increase in reactor coolant temperature and RCS pressure owing to decreased RCS flow; (3) decrease in DNBR owing to increased temperature of reactor coolant; (4) increase in DNBR after occurrence of mDNBR caused by reactor trip and natural circulation. Focusing on the variations in the RCS flow, RCS pressure, and DNBR, a qualitative design validation of the facility was conducted.

The detailed event sequences of two RCP rotor seizure accidents are presented in Table 6. The overall event sequences were referred by those of the APR-1400 final safety analysis (FSAR), and variations in system parameters [23] under RCP rotor seizure condition were compared with the preliminary analysis results, because the APR-1400 FSAR data is not open to public. Stuck of rotors of two RCPs located at different loops initiated the accident, and a low RCS flow rate signal, which corresponded to 80% of the RCS flow rate at the normal operating condition, triggered a reactor trip with a 1.7 s delay. The loss of off-site power (LOOP) condition was assumed to be accompanied by reactor trip. Main feedwater isolation occurred, and the remaining RCPs were tripped.

The RCPs at the loops of 1A and 2A were assumed to be stuck. Owing to two stuck RCP rotors, the total flow rate of the RCS decreased as shown in Fig. 6. Fig. 7 shows the variations in flow rates according to the loops during the simulated RCP rotor seizure accident. The flow rates of two loops (1A and 2A) experiencing rotor seizure were dramatically decreased, whereas the flow rates of the remaining loops (1B and 2B) increased slightly owing to the inertia of the tripped loops (1A and 2A) propagating to the loops

Table 6
Event sequences of two RCP rotor seizure for APR-1400 and URI-LO.

Event	Reference	URI-LO	Remark
Loss of flow (2 RCPs)	0.0 s	0.0 s	
Low RCS flow rate signal	8.6 s	3.0 s	80% of RCS flow rate at full power operation
Reactor trip	10.3 s	3.6 s	Low RCS flow rate signal +1.7 s (0.6 s) delay
LOOP (MFIV and rest RCP trip)	13.3 s	4.7 s	Reactor trip +3.0 s (1.1 s) delay
mDNBR	10.7 s	16.5 s	
Maximum RCS pressure	11.6 s	31.0 s	

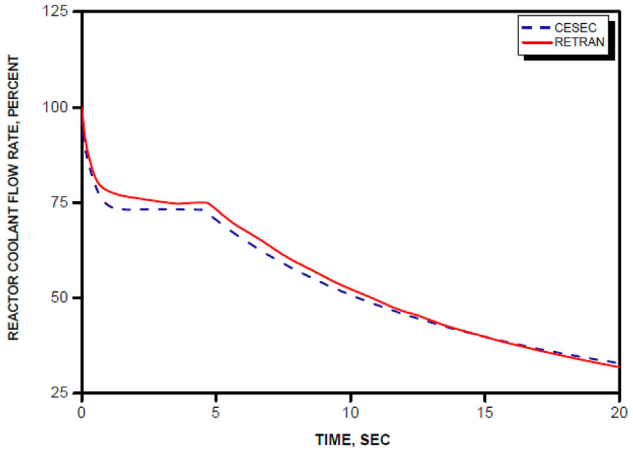

(a) Reference data [23]

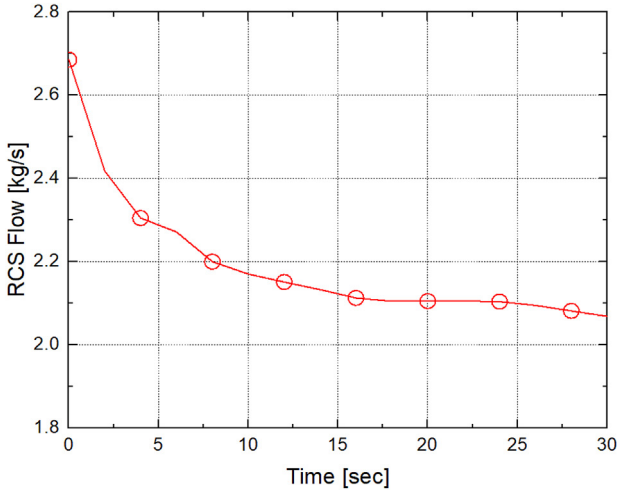

(b) URI-LO

Fig. 6. RCS flow behavior of URI-LO during RCP rotor seizure accident.

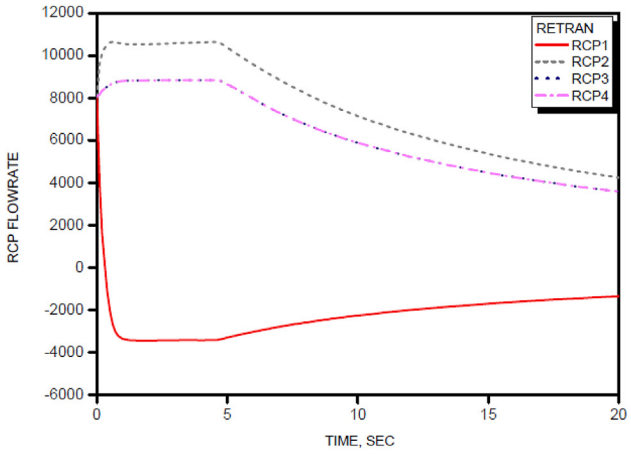

(a) Reference data [23]

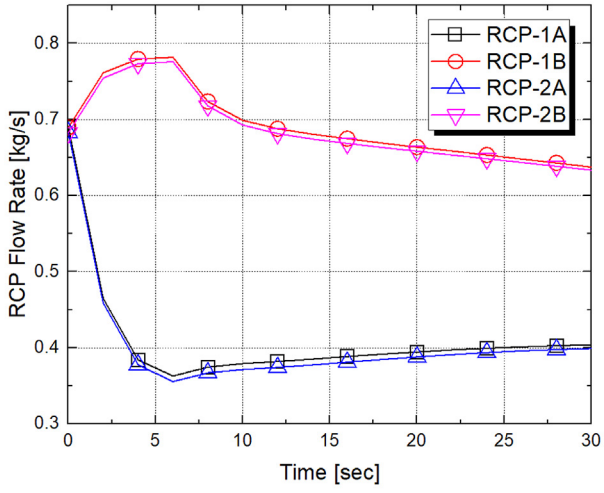

(b) URI-LO

Fig. 7. Variations of RCP flow rates of URI-LO during RCP rotor seizure accident.

until 6 s from initiation of the accident. The remaining RCP trips owing to the occurrence of LOOP induced a decrease in the RCP flow rates at loops 1B and 2B. The time interval between the low RCS flow rate signals of the reference case and the MARS calculation result of this study was attributed to the difference in fluid properties (high-pressure and high-temperature condition of reference case vs. low-pressure and low-temperature condition of the URI-LO) and the scaling effect.

A decrease in the RCS flow rate reduced the heat exchange rate between the RCS and steam generator; consequently, the reactor coolant temperature increased. Therefore, the RCS pressure increased as shown in Fig. 8. The increase in RCS pressure and temperature with reduced RCS flow rate decreased the mDNBR, as depicted in Fig. 9. After the RCS pressure and mDNBR reached their peak and minimum values, respectively, the system pressure decreased and mDNBR increased; as the reduced decay heat from the core decreased, the RCS temperature and void fraction decreased rapidly. The mDNBR and maximum RCS pressures of the URI-LO were longer than the time interval, whereas the reactor trip and LOOP occurred more rapidly compared with the reference case. The reason why the system responses in terms of RCS pressure and mDNBR is initial specific heat of the facility. Although the initial decay heat of the reference power plant was approximately 8%, the

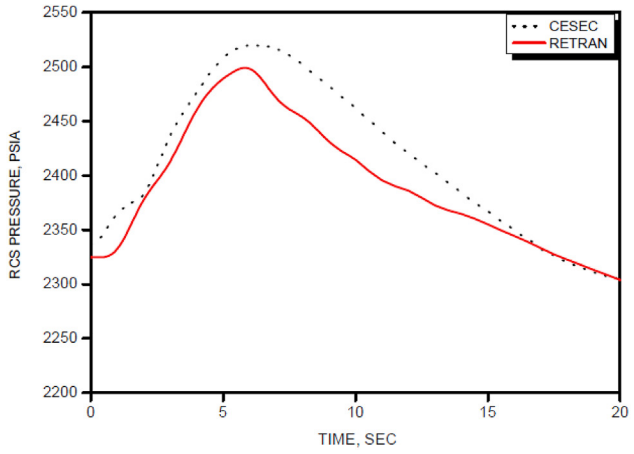

(a) Reference data [23]

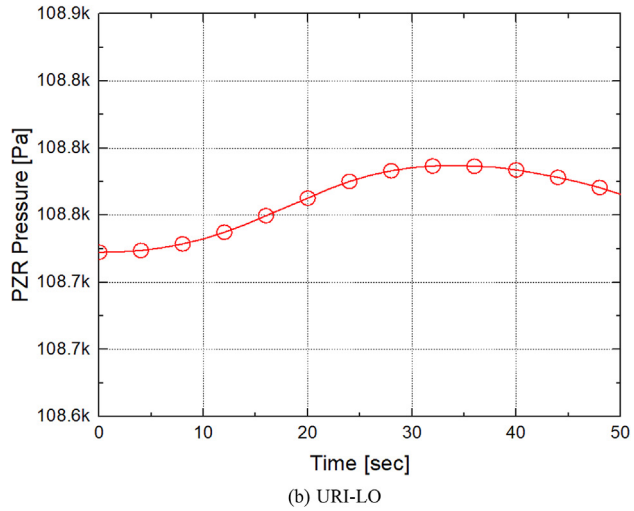

(b) URI-LO

Fig. 8. Variation of RCS pressure of URI-LO during RCP rotor seizure accident.

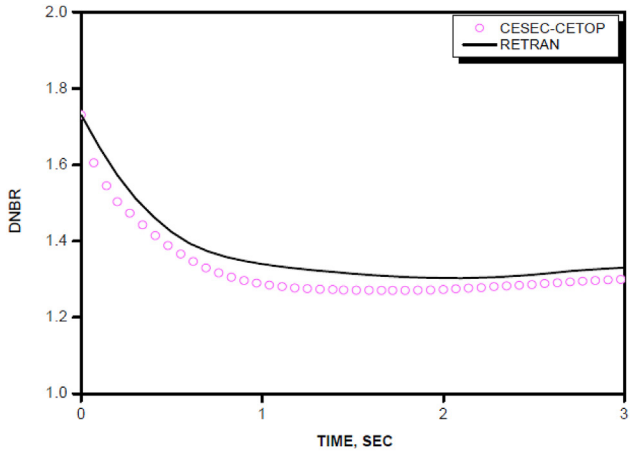

(a) Reference data [23]

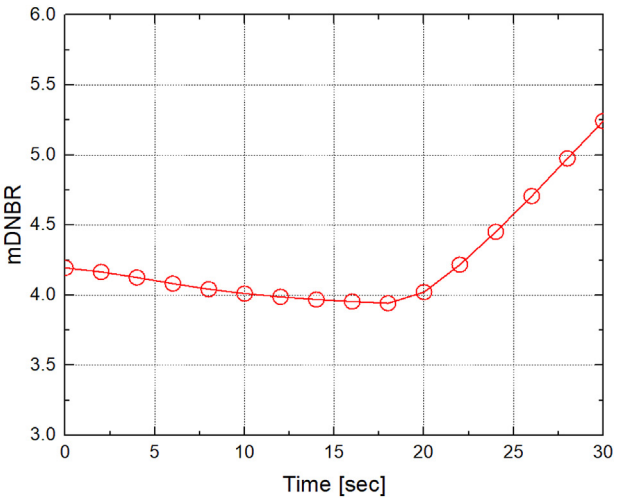

(b) URI-LO

Fig. 9. Variation of mDNBR of URI-LO during RCP rotor seizure accident.

URI-LO can simulate 2% of the reference model's full power. Hence, system responses related to thermal–hydraulic phenomena appeared late in the short-term transient condition. However, it can be concluded that the constructed facility exhibited good simulation performance on short-term transient conditions particularly for RCP rotor seizure accidents, because the system behaviors were reasonably matched with the reference data [13] and qualitatively exhibited specific thermal–hydraulic phenomena (maximum RCS pressure and mDNBR).

3.3. SBO

Even though the simulatability of the URI-LO on short-term transients was proven by preliminary analysis regarding two RCP rotor seizure accidents, most of the postulated transient conditions have been considered in the long-time interval to guarantee reactor safety. Hence, long-term transients must be simulated appropriately as an IET facility. Recently, the SBO after the Fukushima Daiichi accident has been used as a representative postulated accident scenario, and the development of emergency operation plans and passive safety systems to manage prolonged SBOs have become key issues in nuclear safety. The similarity of a facility regarding prolonged SBO can provide insights into the feasibility of newly developing technologies. In this study, the ATLAS SBO-01 test [24,25] was performed to validate the URI-LO design from a long-term transient perspective. The ATLAS facility of the Korea Atomic Energy Research Institute was designed to scale down the APR-1400, and the reference model with the URI-LO was shared. Many IETs have been conducted, which validated the facility design. Therefore, the ATLAS SBO-01 test is a suitable IET to analyze the long-term simulatability of the URI-LO.

The event sequences of the ATLAS SBO-01 and the calculated results of the URI-LO are summarized in Table 7. Owing to the losses of off-site and on-site power, all RCPs and the main feedwater pumps stopped operation with simultaneous reactor trip and main steam isolation. In the transient condition, the decay heat from the core was removed by the SGs and steam was discharged through the MSSVs to secure the integrity of the SGs. Consequently, the coolant inventory of the SGs depleted, and the absence of a heat sink increased the RCS temperature and pressure. As the core water level decreased below the top of the core, the core heat up occurs.

The analyzed system behaviors of the URI-LO under prolonged SBOs are plotted and compared with ATLAS SBO-01 test results as shown in Figs. 10–13. After the initiation of an SBO, the decay heat from the core was removed by the steam generators, and the isolations of the main feedwater and steam resulted in an increase in the SG pressure. When the SG pressures reached the MSSV opening set point, steam was discharged, and the SG pressures decreased.

Table 7
Event sequences of ATLAS SBO-01 and URI-LO.

Event	APR-1400	ATLAS SBO-01	URI-LO
SBO start	0.0 s	0.0 s	0.0 s
RCP/MFP trip	0.0 s	0.0 s	0.0 s
Reactor trip	8.0 s	0.0 s	0.0 s
Turbine trip	9.1 s	0.0 s	0.0 s
SG-1, 2 dryout	2500 s	7500 s	4000 s
PZR full	3050 s	8000 s	4200 s
POSRV 1st opening	~2500 s	8300 s	4000 s
Core heat up	4600 s	10,500 s	6000 s

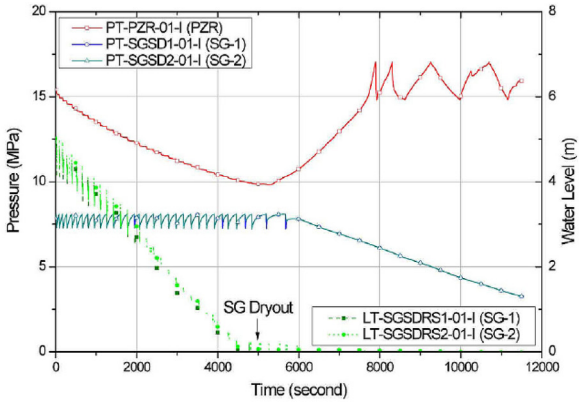

(c) ATLAS SBO-01 [24]

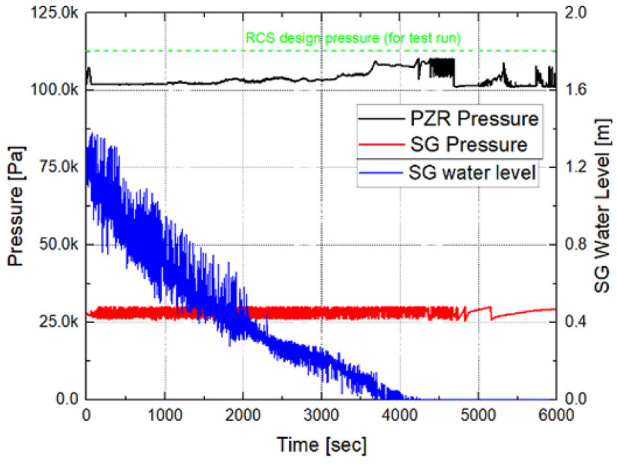

(b) URI-LO

Fig. 10. Changes of system pressures and SG water levels during station blackout.

The repetitive opening and closing of the MSSVs caused an oscillation of SG collapsed water level, as shown in Fig. 10. Eventually, the SG inventory decreased and depleted through the discharge of steam through the MSSVs. As the SG water level decreased, the heat exchange area between the primary and secondary systems as well as the decay heat removal rate through the SGs decreased. The reduced decay heat removal rate increased the RCS pressure, and the depletion of SG inventory accelerated the RCS pressure increase behavior. When the RCS pressure reached the POSRV opening set point (1.07 bar), the reactor coolant was discharged through the POSRV. After the first opening of the POSRV, the RCS pressure oscillated between the pressure boundaries of the POSRV open/close set points. The appropriate operation of the discharge valve ensured that the RCS was maintained below the system design

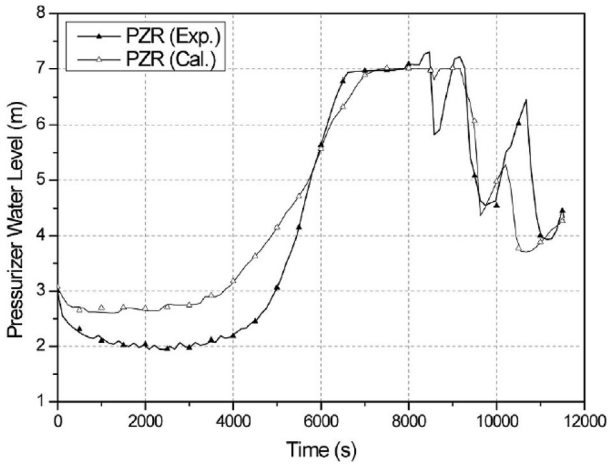

(a) ATLAS SBO-01 [24]

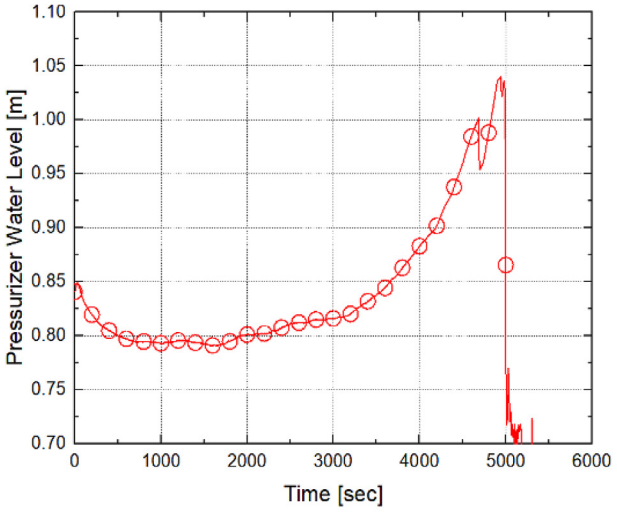

(b) URI-LO

Fig. 11. Variation of pressurizer water level of URI-LO during SBO.

pressure (1.1 bar).

The variation in the collapsed water level of the pressurizer (PZR) during transients is shown in Fig. 11. At the early phase of the transient, a decrease in the core power resulted from the reactor trip decreased the reactor coolant temperature, as shown in Fig. 12. The volume of the reactor coolant decreased with the coolant temperature, and the RCS pressure decreased as well. When the heat removal rate through the SGs was lower than the decay heat, the reactor coolant temperature started to increase and the PZR collapsed water level increased. A time delay was observed between the opening of the POSRV and the PZR water level. During the postulated SBO condition, the upper head of the RPV became saturated and the core level decreased. In this condition, the RPV served as a pressurizer and the PZR a buffer tank. This situation caused a time delay between the operation of the POSRV and the PZR water level, as shown in Figs. 11 and 13. The abovementioned time delay was also observed in the SBO-01 experiment of the ATLAS facility.

In terms of the PZR water level and reactor coolant temperature variations at the end of the transient, the analysis results of the URI-LO and the experimental data differed slightly. The opening of the POSRV induced dramatic decrease of PZR water level, and the core

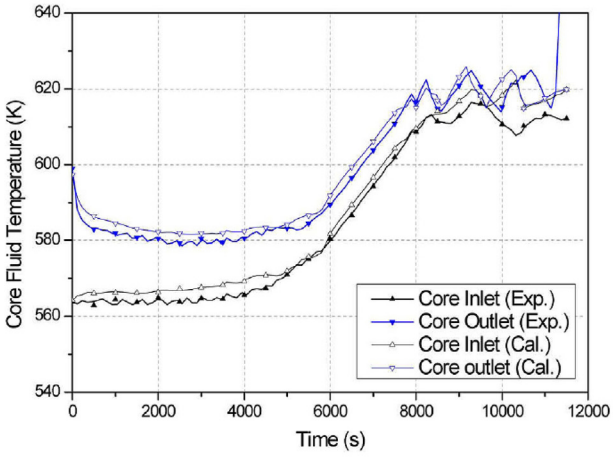

(a) ATLAS SBO-01 [24]

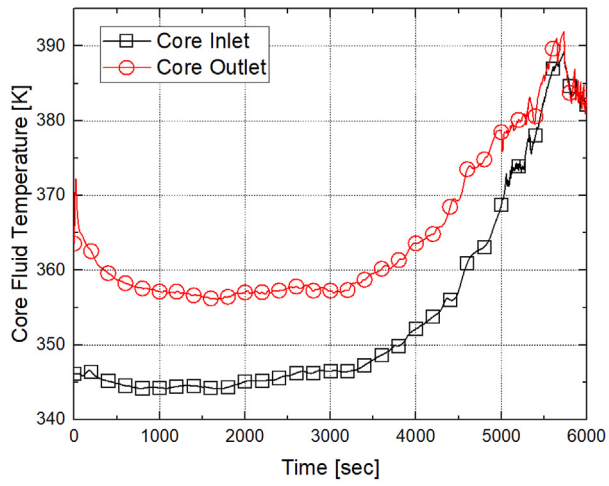

(b) URI-LO

Fig. 12. Core inlet and outlet temperature behavior during SBO.

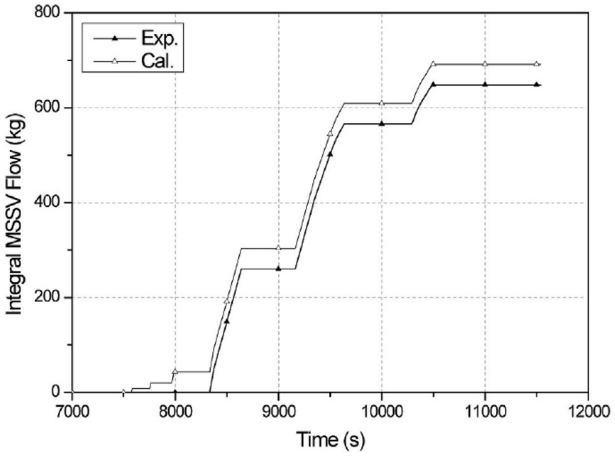

(a) ATLAS SBO-01 [24]

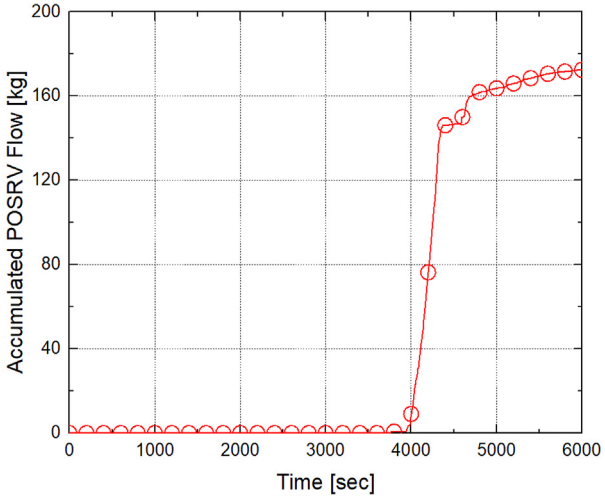

(b) URI-LO

Fig. 13. Variation of accumulated POSRV discharge of URI-LO during SBO.

coolant temperature decreased at the end of the transient condition. Meanwhile, the experimental data showed a lower decrease rate of PZR water level and a continuous increase in the core coolant. The URI-LO had a larger scaling reduction ratio of the PZR suction line and PZR volume compared with that of the ATLAS facility; therefore, the inventory change of the PZR expanded. For the core coolant temperature variation, the total decay heat of the URI-LO during the experimental period could not precisely scale the reference model owing to the maximum power capacity of the facility. The limitations of the URI-LO specified from the preliminary analysis will be preserved using additional scaling designs.

The core water level, RCS flow rate, peak cladding temperature, and other parameters were similar with the experimental data of the ATLAS facility, excluding the abovementioned differences. The difference between event sequences and time interval resulted from the different fluid properties, operating pressure, and temperature, as well as the reduced heat transfer areas of the components. A further analysis using FC-72 simulant will be performed, and the results are expected to agree well with the ATLAS SBO-01 test data quantitatively. Furthermore, it was confirmed that long-term transient system behaviors can be simulated appropriately using the URI-LO. Therefore, base data will be provided for newly suggested passive safety systems, thereby effectively exhibiting their performances in coping with SBOs. Quantitative design validation will be conducted after IETs and further code simulations with simulant fluid properties have been performed.

4. Experimental studies of URI-LO

The main components of an IET facility, such as the heater, RCP, and steam generator, must be validated whether they can function synergistically to exhibit appropriate system behaviors under various operating conditions. In general, physical system behaviors accompanied with specific thermal–hydraulic phenomena are performance indicators of IET facilities. To evaluate the performance and functionality of the facility, a series of experiments was conducted. All the experiments were conducted under the condition where a single steam generator was filled with a coolant (the remaining SG was empty) as a stagnant liquid pool to observe the resolution toward asymmetric behaviors, with fundamental observations on system behaviors.

4.1. Heating test (Natural circulation)

A key element of the IET facility is the heater, which significantly affects the change in system parameters as an energy source. The heater should be controlled within the designed power capacity

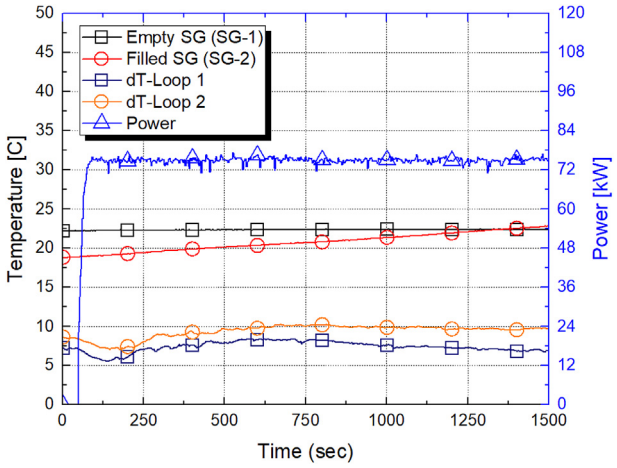

Fig. 14. Variations of temperatures of SGs, temperature differences between hot legs and colds legs according to loops, heat input during heating test.

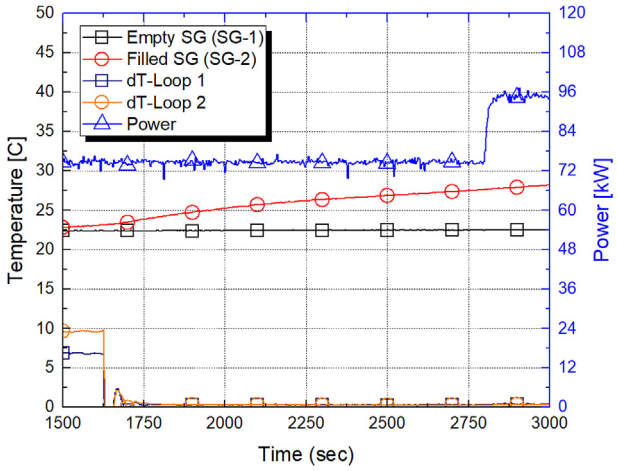

Fig. 15. Variations of temperatures of SGs, temperature differences between hot legs and colds legs according to loops, heat input during transition of natural circulation to forced convection.

range for the simulation of decay heat. Additionally, the operation of an IET facility in the single-phase natural circulation condition is the most important factor supporting the reliability of experimental data, because many transient conditions in the test facility experience an RCP trip. Therefore, a heating test under a natural circulation was performed to assess the facility behaviors under the natural circulation phase.

The heating test results under a single-phase natural circulation is summarized in Fig. 14. In the condition where all the RCPs did not operate and a power of 74 kW was applied to the heater, the temperature difference between the cold and hot legs of the loops, as well as the steam generator temperatures were measured. As shown in Fig. 14, the temperature difference between the cold and hot legs of the loop with a coolant-filled SG (Loop 2) was higher than that of the opposite loop (Loop 1) owing to the different heat removal rates through the steam generators, as proven by the increase in temperature of SG-2 (average of T-SG2-EC and T-SG2-DC in Fig. 4) and the constant temperature of SG-1 (average of T-SG1-EC and T-SG1-DC). In addition, the temperature difference between the cold and hot legs of Loop 2 was nearly constant during the heating test period; by contrast, the temperature difference of Loop 1 decreased owing to the absence of a heat sink. In terms of the reactor coolant flow rate, the flow rate of Loop 2 was higher than that of Loop 1 because a higher buoyancy force of was exerted in Loop 2 owing to a higher temperature difference under an equal height difference between the thermal centers (core and steam generator u-tubes). Although the reactor coolant temperature increased continuously during the test period owing to inefficient heat removal through the SGs, the distinguishable temperature variation and distribution of reactor coolant supported the heating capacity of the heater, simulatability of single-natural circulation, and resolution toward asymmetric loop behaviors. Hence, it was confirmed that the system behaviors inside the URI-LO under natural circulation were valid, and that the facility will have the appropriate simulation capacity for IETs related to natural circulation.

4.2. Forced convection test

RCPs, which circulate the primary system coolant, demonstrates various operation conditions including specific thermal–hydraulic phenomena accompanied with energy generated from a heater. Furthermore, RCPs can rapidly achieve steady-state, change the system temperature and pressure by dominating the convective heat transfer between primary and secondary systems, vary asymmetric operation conditions, and form local thermal–hydraulic phenomena. In addition, forced convection typically reduces the resolutions of system behaviors. The functionality of RCPs and the resolution of system behaviors under forced convection are crucial factors of IET facilities. Therefore, a forced convection test with various RCS flow rates and heat capacities was conducted.

The RCP began to operate based on the heating test condition described in the previous section. The temperatures of the SGs and the temperature difference between the hot and cold legs according to the loops when all of RCPs operated at the same heat input condition with natural circulation were plotted, as shown in Fig. 15. As the coolant flow rate increased by the operation of the RCPs, the temperature increase rate of SG-2 was more significant than that of natural circulation owing to the increased heat exchange rate between the primary and secondary systems through increased convective heat transfer. The reduced reactor coolant temperature with the operation of the RCPs supported the increased heat removal through SG-2, whereas the SG-1 temperature was constant, indicating negligible heat removal. The temperature differences between the cold and hot legs decreased to 0.5 °C owing to increased reactor coolant flow rates, even though that in the natural circulation was 7.3 °C and 9.8 °C, respectively. The change in system behaviors according to experimental conditions is shown in Fig. 16. When the heater power increased to 95 kW, which maintained the RCS flow, the temperature differences between the cold and hot legs of both loops increased. As the RCS flow rate decreased from 40 to 20 kg/s, the temperature differences between the cold and hot leg of the both loops further increased. In addition, the temperature difference between the cold and hot legs of Loop 2 was higher than that of Loop 1 because of the different heat removal rates through the SGs. The distinguishable temperature variation of the loops demonstrated the sufficient resolution of the facility regarding asymmetric system behaviors under certain RCS flow ranges. The RCS flow rate exhibiting a differentiated temperature behavior was higher than that of a predetermined normal operating condition at design analysis. After increasing the coolant flow rate (20–58 kg/s), the temperature differences of the loops converged and became lower than those of other flow rate conditions. Based on the temperatures of steam generators, the heat transfer rates from the primary system to secondary system were calculated. The heat removal rates through SG-1 and 2 were 0.25%

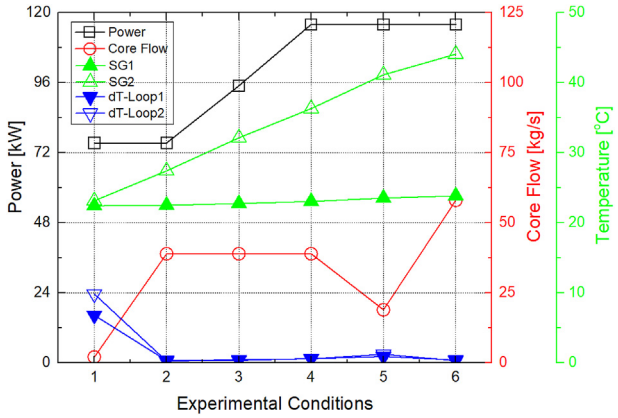

Fig. 16. Variations of system parameters during heating and forced convection tests.

and 4.5%, respectively. Most of rest heat continuously increased the coolant of primary system. Rough heat balance calculation results about core heat, stored energy of primary system coolant, SG heat removal rates, and heat loss indicated that the portion of heat loss was below 10% of core power under the experimental conditions. Although the heat balance between the core and steam generator could not be achieved owing to the poor heat transfer mechanism (convective heat transfer to single-phase liquid pool and atmosphere instead of phase change), asymmetric behaviors were sufficiently observed. For quantitative experiments, the IETs with heat balance between primary and secondary system through forced convection and phase change of coolant at the SGs will be conducted in the future.

The comprehensive data regarding system behaviors under single-phase circulation supported the appropriate test performance of the URI-LO. In addition, it was proven that the URI-LO exhibited sufficient resolution regarding the asymmetric behaviors of the loops, which occurred frequently in various transient conditions. Hence, by observing various system behaviors under the IETs of the URI-LO, the application and performance analysis of innovative technologies are expected to provide reliable data that contribute to the improvement in technical qualities.

4.3. Application of innovative technologies

Plant management and inspection technologies based on 4th industrial revolution technologies is an emerging topic as they can extensively enhance plant operation efficiency and reactor safety (artificial intelligence), design and manufacturing costs (3D printing), and inspection range and reliability (drones and robots). The URI-LO was designed as a micro IET facility to broaden the utilization of IET facilities by providing easy applicability to newly suggested technologies. Hence, the fundamental application of Fourth Industrial Revolution technologies to the URI-LO is being conducted. The current research status regarding the application of innovative technologies is briefly introduced in this section.

Drones are a representative technology of the Fourth Industrial Revolution and are being widely investigated for use in nuclear power plants for inspection and maintenance. To improve their technical quality, a feasibility study involving their use in plant environments is necessitated. In this study, an infra-red (IR)-camera-equipped drone (160 × 120 resolution, 12 μm pixel, and 10% maximum uncertainty from −10 °C–140 °C) was utilized to analyze its feasibility as a plant-inspecting drone. Temperature fields during heating and forced convection tests were obtained during drone aviation, as shown in Figs. 17 and 18. The coolant inventory inside

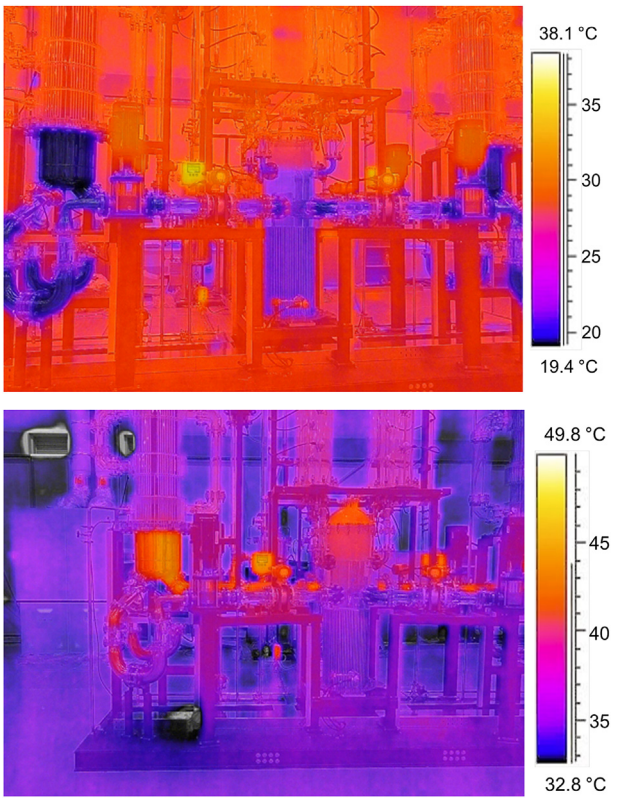

Fig. 17. Temperature field of coolant-filled URI-LO and temperature difference between hot leg and cold legs measured by IR thermometry-equipped drone.

the system including the water level, temperature distribution across the loop, and overall operating condition of the facility were recorded by IR cameras embedded in drone. The IR images exhibited a significant resolution toward the abovementioned operating conditions. Fig. 17 shows the water level of the primary system, providing insights into the measurement of coolant inventory at transient conditions instead of the conventional methodology based on differential pressures in multiple locations. Additionally, the temperature difference between the hot and cold legs was measured using IR images. The temperatures of the RPV upper plenum, RPV upper head, hot legs, and SG lower plenum (red) were clearly distinguished with relatively low-temperature fields (blue) along the intermediate leg, cold leg, and downcomer of the RPV. When the IR image was captured, the temperature difference between the hot and cold legs was 7.3 °C. The resolution enables an operator to assess the system condition rapidly and reduce the coping time against off-normal conditions and accidents. Fig. 18 depicts the temperature field of the entire system. The observed temperature field of SG 1 was approximately the room temperature, and the SG-2 temperature was higher than 35 °C. As shown in Fig. 18, the operation of a single SG (SG-2) and the malfunctioning of SG-1 (asymmetric operation) can be distinguished.

The applicability of drones for nuclear power plants was briefly evaluated, and the results indicated it can be utilized as an inspection device by based on measurements of temperature field, leaking coolant, visual data, etc. The drone can aviate to various positions and measure local/global temperature fields; however, many issues, such as internal temperature variations, material effect, data reliability, and automatic aviation still exist. In the future, studies utilizing drones in plant environments will be performed and continuously evaluated.

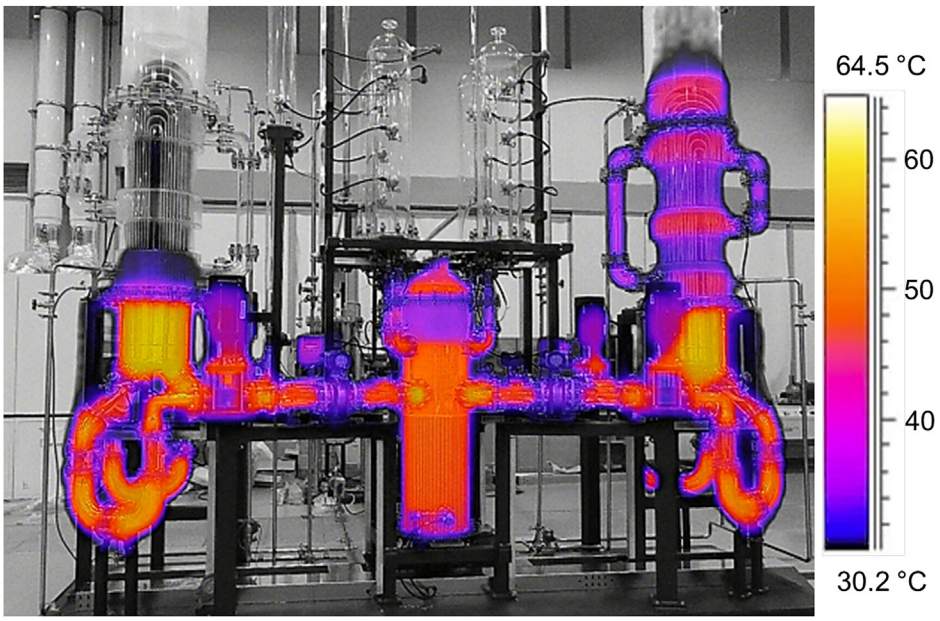

Fig. 18. Temperature filed of URI-LO during forced convection test.

4.4. Future studies

A qualitative design analysis on the constructed URI-LO was conducted based on a series of code analysis and experiments. The analysis results showed that the URI-LO possessed sufficient capacity in demonstrating appropriate system behaviors, and thermal–hydraulic phenomena occurred in the reference model. The facility operation and the introduction of advanced technology at the facility exhibited the performance as the IET facility and its possible contribution to nuclear engineering. However, the URI-LO must be quantitatively validated, because it exhibited noticeable reduction scales and utilization of simulant fluid, which have not been studied in IET facility design. Several specific phenomena, such as discharge flow through safety valves, flashing, flow instability, countercurrent flow, flow pattern transition, and enthalpy change with elevations are expected to be distorted owing to different property changes between water and the simulant fluid, as well as the pressure difference between the system and environment. Even though the characteristics of the URI-LO can induce scaling distortions in terms of specific thermal–hydraulic phenomena, an investigation of the distortion effects would contribute to the improvement in the scaling analysis methodology through the development of preservation methods. For a quantitative design validation of the URI-LO, IETs predetermined in the design process will be performed using a simulant fluid. The IET results and scaling analysis method will be converted to system behaviors of a reference model (APR1400). The converted data will be compared with numerical analysis results based on the MARS code and reference experimental data. In the phase of comparison between experimental data and code analysis results, heat loss characteristics of facility and validity of MARS model (including nodalization of URI-LO) will be evaluated for high prediction capability of the code on facility behaviors under various IETs. This process will enable the scaling distortion effects to be deduced and the URI-LO design to be validated. Design validation is essential for proving the experimental data of a test facility and the evaluation of various technologies. After proving the facility design, the experimental range of URI-LO will be extended to broaden its utilization and performance.

Because the URI-LO was designed to be utilized as a test facility for innovative technologies, technologies currently developed based on Fourth Industrial Revolution technologies, such as drones, 3D printing, artificial intelligence (AI), IOT, and advanced sensing techniques will be applied to the facility and their feasibility will be evaluated. Several parts of the URI-LO that are difficult to be manufactured by conventional hardware or have many welding parts will be fabricated using a 3D printer. In addition, big data produced by IETs will be provided in the development of reliable AI, for example, decision-making support systems, virtual reactors, and malfunction sensing systems. Based on the abovementioned plans, innovative technologies will be continuously adopted to the facility and performance tests will be performed.

5. Conclusions

A micro IET facility, i.e., the URI-LO, was designed and constructed as a test bed for new innovative technologies. Based on a three-level scaling approach, the URI-LO was designed to exhibit significantly reduced scales of 1/8 height ratio and 1/12 diameter ratio with respect to APR-1400. In particular, transparent components comprising the facility improved the understanding of various system behaviors and thermal–hydraulic phenomena through visualization data. The utilization of simulant fluids and the appropriate scaling analysis yielded the similarity of high-pressure and high-temperature conditions of a reference model with low-pressure and low-temperature conditions. To evaluate the performance of the URI-LO as an IET facility, preliminary analyses using the MARS-KS code were conducted for RCP rotor seizure accidents and prolonged SBOs. Safety analysis results regarding the reference model and the experimental data of the ATLAS facility sharing prototype of the URI-LO were compared with preliminary analysis results. The calculation results qualitatively proved the simulatability of the facility for short- and long-term transients, showing similar system behaviors with the reference data. Subsequently, a series of experiments for observing the functionality of the test facility was conducted. Natural circulation and forced convection behaviors observed under various heat inputs and flow rates were physically valid, exhibiting sufficient resolutions

regarding the asymmetric system behaviors. Therefore, the IETs of the URI-LO are expected to contribute to the improvement in the technical quality of innovative technologies based on Fourth Industrial Revolution technologies by providing reliable data that enable easy applications. In the future, the URI-LO design will be quantitatively validated through various IETs using simulant fluids and numerical analysis. Consequently, the performances and feasibility tests of newly suggested technologies will be evaluated using the URI-LO, and their applications to nuclear power plants will afford reactor safety and operation efficiency.

Declaration of competing interest

The authors declare that they have no known competing financial interests or personal relationships that could have appeared to influence the work reported in this paper.

Acknowledgement

This work was supported mainly by Korea Hydro & Nuclear Power Company through the project “Nuclear Innovation Center for Haeorum Alliance" and partly by the Korea Institute of Energy Technology Evaluation and Planning (KETEP) and the Ministry of Trade, Industry & Energy (MOTIE) of the Republic of Korea (No. 20194030202400).

References

[1] M. Kasamatsu, S. Hanada, E. Noda, Development of the decision make supporting system on incident management, in: International Congress on Advances in Nuclear Power Plants, Fukui and Kyoto, Japan, April 24-28, 2017.
[2] H.S. Cho, T.H. Woo, Mechanical analysis of flying robot for nuclear safety and security control by radiological monitoring, Ann. Nucl. Energy 94 (2016) 138–143.
[3] J.S. Kim, Y.H. Jang, Development of stable walking robot for accident condition monitoring on uneven floors in a nuclear power plant, Nucl. Eng. Tech. 49 (2017) 632–637.
[4] M.V. de Oliveira, J.C.S. de Almeida, Application of artificial intelligence techniques in modeling and control of a nuclear power plant pressurizer system, Prog. Nucl. Energy 63 (2013) 71–85.
[5] K. Hagita, Y. Kodama, M. Takada, Simplified virtual training system for radiation shielding and measurement in nuclear engineering, Prog. Nucl. Energy 118 (2020) 103127.
[6] I.J.A.L. Santos, C.H.S. Grecco, A.C.A. Mol, P.V.R. Carvalho, The use of questionnaire and virtual reality in the verification of the human factors issues in the design of nuclear control desk, Int. J. Ind. Ergon. 39 (2009) 159–166.
[7] S.H. Kim, S.H. Chang, Y.J. Choi, Y.H. Jeong, A passive decay heat removal strategy of the integrated passive safety system (IPSS) for SBO combined with LOCA, Nucl. Eng. Des. 295 (2015) 346–359.
[8] Y.S. Jeong, K.M. Kim, I.G. Kim, I.C. Bang, Hybrid heat pipe-based passive in-core cooling system for advanced nuclear power plant, Appl. Therm. Eng. 90 (2015) 609–618.
[9] S.D. Park, I.C. Bang, Feasibility of flooding the reactor cavity with liquid gallium coolant for IVR-ERVC strategy, Nucl. Eng. Des. 258 (2013) 13–18.
[10] G.G. Loomis, Summary of the semiscale program (1965-1986), Idaho Natl. Eng. Lab. (1987). NUREG/CR-4945.
[11] M. Bacchiani, C. Medich, M. Rigamonti, SPES-2, the full-height, full-pressure test facility simulating the AP600 plant, comparison among 2” CL to core make-up tank pressure balance line break, in: Fifth International Topical Meeting on Nuclear Thermal Hydraulics, Operation and Safety, 1997. Beijing, China, April 14-18.
[12] K. Umminger, L. Dennhardt, s. Schollenberger, Integral test facility PKL: experimental PWR accident investigation, Sci. Technol. Nucl. Instal. (2012) 891056, 2012.
[13] A. Prosek, O.A. Berar, Advanced presentation of BETHSY 6.2TC test results calculated by RELAP5 and TRACE, Sci. Tech. Nucl. Instal. (2012) 812130, 2012.
[14] D.L. Reeder, Loft system and test description (5.5-rt nuclear core 1 LOCES), Idaho. Natl. Eng. Lab. (1978). NUREG/CR-0247.
[15] Y. Kukita, K. Takasa, H. Asaka, T. Yonomoto, H. Nakamura, The effects of break location on PWR small break LOCA: experimental study at the ROSA-IV LSTF, Nucl. Eng. Des. 122 (1990) 255–262.
[16] M. Ishii, S.T. Ravankar, R. Dowlati, M.L. Bertodano, I. Babelli, W. Wang, H. Pokhama, V.H. Ransom, R. Viskanta, T. Wilmarth, J.T. Han, Scientific Design of Purdue University Multi-Dimensional Integral Test Assembly (PUMA) for GE SBWR, NRC, 1996. NUREG/CR-6309.
[17] J.N. Reyes, Scaling Analysis for the OSU APEX-CE Integral System Test Facility, Oregon State University, 2001. NUREG/CR-6731.
[18] Y.-S. Kim, K.Y. Choi, H.S. Park, S. Cho, B.D. Kim, N.H. Choi, W.P. Baek, Commissioning of the ATLAS thermal-hydraulic integral test facility, Ann. Nucl. Energy 35 (2008) 1791–1799.
[19] M. Ishii, I. Kataoka, Scaling laws for thermal-hydraulic system under single phase and two-phase natural circulation, Nucl. Eng. Des. 258 (1984) 411–425.
[20] W.A. Carbiener, R.A. Cudnik, Similitude considerations for modeling nuclear reactor blowdowns, Trans. Am. Nucl. Soc. 12 (1969) 361–362.
[21] A.N. Nahavandi, F.S. Castellana, E.N. Moradkhanian, Scaling laws for modeling nuclear reactor system, Nucl. Sci. Eng. 72 (1979) 75–83.
[22] K.M. Kim, I.C. Bang, Integral effect tests in visualization basis 3D printed test facility for improved applicability of innovative technologies, in: International Topical Meeting on Nuclear Reactor Thermal Hydraulics, 2019. Portland, OR, USA, Aug. 18-23.
[23] H.J. Yoon, Y.H. Kim, D.H. Lee, C.K. Seong, A safety analysis of the locked rotor event for Ulchin unit 3/4 using RETRAN code, in: Transaction of 2004 KNS Spring Meeting, 2004. Gyeongju, Korea, March 27-28.
[24] Y.S. Kim, S.G. Yu, K.H. Kang, H.S. Park, S. Cho, K.Y. Choi, Analysis of a station blackout scenario with an ATLAS test, Nucl. Eng. Tech. 45 (2013) 179–190.
[25] X.G. Yu, H.S. Park, Y.S. Kim, K.H. Kang, S. Cho, K.Y. Choi, Systematic analysis of a station blackout scenario for APR1400 with test facility ATLAS and MARS code from scaling viewpoint, Nucl. Eng. Des. 259 (2013) 205–220.